IJASRaR International Journal of Applied Sciences and Radiation Research
ISSN: 3062-2751
www.ijasrar.com ijasrar@gmail.com
Vol. 3-No.1 (2026) pp. 22-33
Research Article

Nuclear Technologies Social Science Focus: Public perception and socio-political attitudes toward nuclear energy, medical isotopes, and radiation safety

Demet Sariyer*

Manisa Celal Bayar University, Turgutlu Vocational High School, Turgutlu, Manisa, Turkey
* **Corresponding Author Email:** demet.sariyer@cbu.edu.tr - **ORCID:** 0000-0002-7803-111X

Article History:

DOI: 10.22399/ijasrar.64
Received: March 12, 2026
Revised: May. 20, 2026
Accepted: May. 23, 2026

Keywords:

Proton accelerator;
Underground shielding;
FLUKA Monte Carlo;
Secondary particle production;
Neutron moderation;
Ferroboron shielding

Abstract: Radiation safety in underground proton accelerator facilities depends not only on the determination of adequate shielding thicknesses but also on the accurate modeling of secondary particle production, transport, and interactions within shielding materials. While most previous studies have primarily focused on ambient dose equivalent or particle fluence distributions, investigations simultaneously addressing secondary particle production, particle stopping processes within shielding systems, and low-energy neutron moderation remain limited. In this study, a three-dimensional underground proton accelerator tunnel was modeled using the FLUKA Monte Carlo (MC) particle transport code. The computational model incorporated a multilayer ferroboron (FeB)-concrete shielding system surrounded by natural soil, and the radiation field generated by the interaction of a monoenergetic 250 MeV proton beam with a copper target was comprehensively investigated. Secondary particle production yields, the distributions of particles completely stopped within the shielding materials, and low-energy neutron-induced interactions were analyzed simultaneously to provide a comprehensive physical interpretation of radiation transport mechanisms. The results revealed that approximately 85% of all generated secondary particles consisted of protons, neutrons, and photons, indicating that these three particle species dominate the radiation field. Furthermore, the multilayer FeB-concrete shielding system was found to effectively attenuate charged particles through ionization energy loss and nuclear interactions, whereas low-energy neutron transport was governed predominantly by elastic scattering processes. The surrounding natural soil was also shown to enhance neutron moderation through multiple scattering mechanisms, functioning as an additional passive biological shielding layer alongside the engineered shielding system. Overall, this study provides a comprehensive understanding of the fundamental physical processes governing radiation fields in underground proton accelerator facilities and offers valuable guidance for the optimization of multilayer shielding systems as well as the radiation-safe design of future proton therapy and accelerator research facilities.

1. Introduction

The rapid expansion of high-energy proton accelerator applications in recent years has made comprehensive radiation safety assessments an essential requirement for these facilities [1-8]. In particular, many modern accelerator installations, including proton therapy centers, research laboratories, and particle physics facilities, are constructed underground to minimize environmental radiation exposure, enhance structural safety, and optimize land utilization [1-3]. In such facilities, the concrete tunnel structure, together with the surrounding natural soil, forms a multilayer shielding system. Consequently, accurate radiation shielding assessments require not only the evaluation of engineered shielding materials but also a detailed investigation of the influence of the surrounding geological environment on secondary radiation transport [1-3].The interaction of proton beams with target materials and accelerator components generates a wide variety of secondary particles. Among these, neutrons constitute the most critical radiation component governing shielding design because of their electrically neutral nature, broad energy spectrum, and high penetration capability [9-15]. As they propagate through concrete walls, the roof, the floor, and the surrounding soil, neutrons undergo numerous elastic and inelastic interactions, resulting in significant modifications of their energy spectra. Accurate modeling of these transport processes is therefore essential for the reliable prediction of both occupational radiation exposure and environmental radiation levels surrounding accelerator facilities [1-3].Concrete structures employed in underground accelerator facilities play a crucial role in neutron moderation and scattering, while the surrounding soil serves as an additional natural shielding layer [1-3,13]. Material properties of the soil, including its density, chemical composition, and hydrogen content, directly influence neutron transport and contribute significantly to the slowing down and absorption of low-energy neutrons. Furthermore, multiple scattering processes occurring within the soil may lead to the redistribution of neutrons over specific energy ranges. Therefore, the combined evaluation of concrete and soil layers is indispensable for reliable shielding analyses that accurately represent the operational conditions of underground accelerator facilities [11,13,16].Experimental investigations in accelerator shielding studies are not always feasible because of their high cost, limited accessibility, and radiation safety constraints. Consequently, Monte Carlo (MC)-based particle transport simulations have become one of the most reliable approaches for accurately modeling particle interactions in complex geometries. Among the available MC codes, FLUKA is extensively employed in radiation shielding analyses of proton accelerators owing to its capability to simulate high-energy hadronic interactions, electromagnetic processes, and low-energy neutron transport down to thermal energies within a unified and experimentally validated physics framework. Studies performed using FLUKA have made significant contributions to the literature by enabling comparative evaluations of shielding materials, accurate calculations of ambient dose equivalent distributions, and detailed characterization of neutron energy spectra [17-25].A review of the existing literature reveals that most studies have focused on evaluating the radiation attenuation performance of single-material shielding systems, whereas comparatively fewer investigations have addressed the design and optimization of multilayer shielding configurations [11-15,21-23]. Furthermore, the majority of studies on multilayer shielding have been conducted for above-ground proton accelerator facilities [12,25-28]. In contrast, investigations simultaneously examining secondary particle production, particle stopping within shielding materials, and the generation of low-energy neutrons through moderation in underground proton accelerator facilities surrounded by natural soil remain scarce. Most existing studies primarily evaluate shielding performance in terms of total dose or particle fluence, without providing a comprehensive analysis of how underground geometry and the surrounding natural soil influence secondary particle production, particle absorption, and low-energy neutron generation. Consequently, a significant knowledge gap remains regarding radiation safety and shielding optimization for underground proton accelerator facilities [1-3].In multilayer shielding systems, the material type, layer thickness, and stacking sequence collectively determine neutron attenuation performance [12,25-28]. Consequently, hybrid shielding structures incorporating different materials have attracted increasing attention in recent years. Yani et al. (2026) demonstrated that concrete–iron and concrete-polyethylene multilayer configurations provide superior radiation attenuation compared with conventional single-layer concrete shields [26]. Aliyah (2024) reported that multilayer shielding structures can reduce the overall shielding thickness by approximately 25-40% while maintaining effective radiation protection [27]. Sarıyer and Küçer (2018) investigated a multilayer concrete-iron shielding configuration for an above-ground proton accelerator facility and showed that the addition of an iron layer behind the concrete significantly enhanced the attenuation of high-energy neutrons [25]. Similarly, Fang et al. (2025) analyzed a concrete-iron-concrete sandwich shielding structure for an above-ground proton therapy facility using FLUKA MC simulations and demonstrated that the multilayer configuration reduced the transmitted secondary neutron dose by approximately a factor of two compared with a concrete wall of the same thickness [28]. More recently, Sarıyer and Erbil (2026) compared several multilayer concrete-iron shielding arrangements for a 50 MeV above-ground proton accelerator and demonstrated that the layer sequence has a decisive influence on both secondary particle production and spatial dose distributions [12].Despite these advances, previous studies have been almost exclusively devoted to above-ground accelerator facilities. To the best of our knowledge, a comprehensive investigation of secondary particle production, particle stopping mechanisms, and low-energy neutron moderation in a multilayer FeB-concrete shielding system embedded within a natural underground environment has not yet been reported. The present study addresses this gap by employing FLUKA MC simulations to investigate the coupled effects of multilayer engineered shielding and surrounding natural soil on radiation transport in an underground 250 MeV proton accelerator facility, thereby providing new insights into shielding optimization and radiation safety for future underground accelerator installations.Ensuring radiation safety in underground proton accelerator facilities requires not only the determination of appropriate shielding thicknesses but also the accurate modeling of particle transport within the underground geometry and the surrounding natural environment. Consequently, only a limited number of MC-based studies have focused on the shielding design of underground accelerator facilities in recent years. One of the earliest comprehensive investigations was conducted by Sasamoto et al. (2002), who evaluated the radiation field generated by high-power proton beams for the shielding design of the Japan Proton Accelerator Research Complex (J-PARC). Their study examined an underground shielding concept incorporating both concrete and natural soil for a facility consisting of a 600 MeV linear accelerator and 3 GeV and 50 GeV proton synchrotrons. The authors demonstrated that locating the facility approximately 10 m below ground provides significant advantages by allowing the surrounding natural soil to function as an additional biological shielding layer. They also emphasized that shielding constitutes one of the major cost components of high-power proton accelerator facilities and that MC simulations play a crucial role in the development of reliable shielding designs [1].Subsequently, Mueller and Stevenson (2005) performed a detailed shielding assessment of the underground experimental area at Point 5 of the CERN Super Proton Synchrotron (SPS) using FLUKA MC simulations. Their study investigated the adequacy of the concrete shielding separating adjacent experimental halls under increased proton beam intensities and demonstrated that the approximately 4.8 m thick primary concrete shielding satisfied the prescribed design dose limits. However, radiation leakage was observed through penetrations such as access corridors and service ducts, highlighting that shielding evaluations for underground accelerator facilities should address not only the primary shielding walls but also geometric openings and penetration regions that may significantly influence radiation transport [2].Approximately two decades later, DiJulio et al. (2022) carried out comprehensive radiation transport analyses for the European Spallation Source (ESS) linear proton accelerator. Using FLUKA-based simulations, they investigated the radiation field generated by a 2 GeV, 5 MW proton beam and evaluated the combined shielding performance of thick concrete structures and the surrounding natural soil. Their results demonstrated that radiation streaming through service ducts, cable penetrations, and other structural openings can significantly affect shielding effectiveness. Furthermore, they emphasized that reliable radiation protection assessments should consider not only prompt radiation but also activation processes during facility design [3].Collectively, these studies indicate that shielding research for underground proton accelerator facilities has primarily focused on dose distributions, shielding thickness optimization, radiation leakage through penetrations, and activation analyses. However, comprehensive investigations addressing the physical relationship between secondary particle production resulting from proton-target interactions, particle stopping within multilayer shielding systems, and low-energy neutron moderation in underground proton accelerator facilities surrounded by natural soil remain extremely limited. Most existing studies evaluate shielding performance primarily in terms of total dose or particle fluence, without providing a detailed analysis of how underground geometry and the surrounding geological environment influence secondary particle production, particle absorption, and low-energy neutron generation.

To address this gap, the present study employs the FLUKA MC particle transport code to develop a detailed three-dimensional model of a 250 MeV underground proton accelerator facility. The effects of a multilayer FeB-concrete shielding system and the surrounding natural soil on secondary particle production, particle stopping processes, and low-energy neutron transport are investigated within a unified physical framework. By simultaneously examining these fundamental radiation transport mechanisms, this study extends beyond conventional dose-based evaluations and provides new insights into the physical processes governing radiation fields in underground proton accelerator facilities, thereby contributing to the optimization of multilayer shielding systems and the radiation-safe design of future underground accelerator installations.The principal novelty of the present study lies in the comprehensive evaluation of the contribution of the surrounding natural soil to radiation shielding performance in a fully underground proton accelerator facility by investigating the mechanisms of secondary particle production resulting from proton-target interactions. In particular, the production yields of neutrons, photons, protons, and other secondary particles, the fractions of particles completely stopped within the shielding system, and the contribution of low-energy neutrons generated through moderation to the total neutron population were analyzed simultaneously. This integrated approach provides a quantitative assessment of the influence of the surrounding natural soil on particle transport and neutron moderation processes.To achieve this objective, a three-dimensional model of a fully underground proton accelerator tunnel was developed using the FLUKA MC particle transport code, and the particle production mechanisms resulting from the interaction of a 250 MeV proton beam with a copper target were investigated in detail. Particle transport through the multilayer FeB-concrete shielding system, including the side walls, roof, floor, and the surrounding natural soil, was comprehensively analyzed. Secondary particle production yields, particle stopping fractions, and low-energy neutron generation were evaluated simultaneously to quantitatively determine the additional shielding contribution provided by the natural soil. The findings are expected to improve the understanding of the shielding role of natural soil in underground proton therapy centers and accelerator research facilities, enhance radiation safety assessments, and provide a valuable scientific basis for the optimization of shielding designs in future underground proton accelerator installations.

2. Materias and Methods

2.1 MC Simulation Method

The MC simulations performed in this study were carried out using the **FLUKA MC particle transport code,** which is widely employed in particle transport and radiation shielding analyses. FLUKA is capable of simulating the transport of hadrons, neutrons, photons, electrons, heavy ions, and other particle species over a broad energy range using experimentally validated physical models. Owing to its ability to accurately model hadronic interactions, electromagnetic processes, low-energy neutron transport, and secondary particle production, FLUKA has been extensively applied in accelerator physics, radiation protection, medical physics, and radiation shielding design.To ensure the transparency and reproducibility of the computational model, the FLUKA input file was organized in a modular structure comprising geometry definitions, material specifications, particle source configuration, physics models, detector (scoring) definitions, and simulation control parameters. The principal FLUKA input cards employed in the simulations and their corresponding functions are summarized in **Table 1.**

Table 1. *Principal FLUKA input cards employed in the MC simulations and their corresponding functions.*

Simulation Component	FLUKA Cards	Function
Geometry definition	GEOBEGIN, SPH, RPP, END	Accelerator tunnel, shielding structures, concrete base, roof, air and soil
Region definition	REGION	Boolean construction of physical regions
Material definition	MATERIAL, COMPOUND	Material compositions and densities
Material assignment	ASSIGNMA	Assignment of materials to regions
Beam definition	BEAM, BEAMPOS	1000 MeV proton source

Physics models	DEFAULTS (SHIELDIN), PHYSICS	Hadronic, electromagnetic and neutron transport
Material transport	STERNHEIMER, MAT-PROP	Energy-loss and transport corrections
Random numbers	RANDOMIZE	Independent simulation cycles
Dose scoring	USRBIN	Ambient dose equivalent H*(10)
Simulation control	START, STOP	Execution of MC histories

The accelerator geometry was constructed using the **Combinatorial Geometry (CG)** approach implemented in the FLUKA code. The outer boundaries of the computational domain were defined using spherical surfaces (SPH), whereas the accelerator tunnel, multilayer shielding structures, concrete roof, concrete floor, surrounding air region, and natural soil were modeled using rectangular parallelepipeds (RPPs). The physical regions were subsequently generated through Boolean operations and defined using the **REGION** cards. This approach enabled independent particle transport calculations within each material region.The physical properties of the shielding materials were specified using the **MATERIAL** and **COMPOUND** cards. Each material was defined according to its elemental composition and mass density reported in the literature. The materials were then assigned to their corresponding geometric regions using the **ASSIGNMA** cards, thereby completing the material distribution required for the particle transport calculations.The particle source was defined using the **BEAM** and **BEAMPOS** cards. In the simulations, a monoenergetic **250 MeV proton beam** was directed toward a copper target located within the computational geometry. Copper was selected as the target material because of its high secondary particle production yield resulting from proton-nucleus interactions. The incident proton beam was oriented along the positive *z*-axis toward the target.Particle transport calculations were performed using the **DEFAULTS = SHIELDIN** physics setting. This predefined physics configuration includes comprehensive models for hadronic interactions, electromagnetic processes, intranuclear reactions, and low-energy neutron transport. Consequently, secondary particle production arising from proton-target interactions, neutron moderation, scattering mechanisms, and particle transport through the multilayer shielding system were simulated using experimentally validated physical models.The radiation fields were evaluated using three-dimensional **USRBIN (DOSE-EQ)** scorers. The USRBIN detectors were defined on a Cartesian mesh to calculate the ambient dose equivalent, *H**(10), throughout the computational domain. This approach enabled the detailed determination of the spatial dose distributions within the accelerator tunnel, the multilayer shielding system, and the surrounding natural soil.All MC simulations were performed on a local workstation. To reduce statistical uncertainties, **five independent simulations** were conducted, each employing **2×10^7 primary protons,** resulting in a total of **1×10^8 particle histories.** Density-effect and energy-loss corrections were implemented using the **STERNHEIMER** and **MAT-PROP** cards, while independent random-number seeds were generated for each simulation using the **RANDOMIZE** card. Finally, the results obtained from the five independent simulations were statistically combined to reduce stochastic fluctuations and improve the reliability of the calculated dose distributions.

3. Underground Accelerator Geometry and Shielding System

A three-dimensional computational geometry representing an underground proton accelerator facility was developed using the **CG** approach implemented in the FLUKA MC particle transport code. The geometry was constructed using RPPs combined with Boolean operations and comprised the accelerator tunnel, the multilayer shielding system, and the surrounding natural geological environment. The computational model was designed to realistically represent an underground accelerator facility, with the tunnel being completely embedded within the surrounding natural soil, including the roof, floor, and lateral sides.The accelerator tunnel was modeled as a rectangular air-filled structure. The tunnel geometry extended from **−250 cm to +250 cm** along the *x*-axis, **0 cm to 500 cm** along the *y*-axis, and **−500 cm to +500 cm** along the *z*-axis. A copper target with approximate dimensions of **$5 \times 5 \times 5$ cm³** was positioned at the center of the tunnel, and a monoenergetic proton beam was directed toward the geometric center of the target along the positive *z*-axis. The transport of secondary particles generated through proton-nucleus interactions within the copper target was investigated in detail using this computational geometry. **Figure 1** illustrates the three-dimensional computational model of the underground proton accelerator tunnel, including the centrally positioned copper target and the surrounding multilayer shielding system. Side shielding structures were defined on both sides of the accelerator tunnel, consisting of the **FeB side shielding (Wall 1)** and the **concrete side walls (Walls 2 and 3).** In addition, a **concrete roof shield (Wall 4)** and a **concrete floor shield (Wall 5)** were incorporated into the model. Consequently, the accelerator tunnel was completely enclosed by a multilayer shielding system in all four directions. The tunnel interior was modeled as an air-filled region in which particle transport takes place, while the shielding layers were arranged symmetrically around the tunnel to ensure a realistic representation of the shielding configuration. To reproduce underground operating conditions, the entire volume surrounding the accelerator tunnel was modeled as **natural soil.** The soil region extended to the outer boundary of the computational domain, thereby representing the geological environment encountered in actual underground proton accelerator facilities. This modeling approach enabled the moderation, multiple scattering, and energy-loss processes experienced by secondary particles after traversing the engineered shielding layers to be realistically simulated within the surrounding soil. Consequently, environmental neutron transport was evaluated under physically representative boundary conditions.

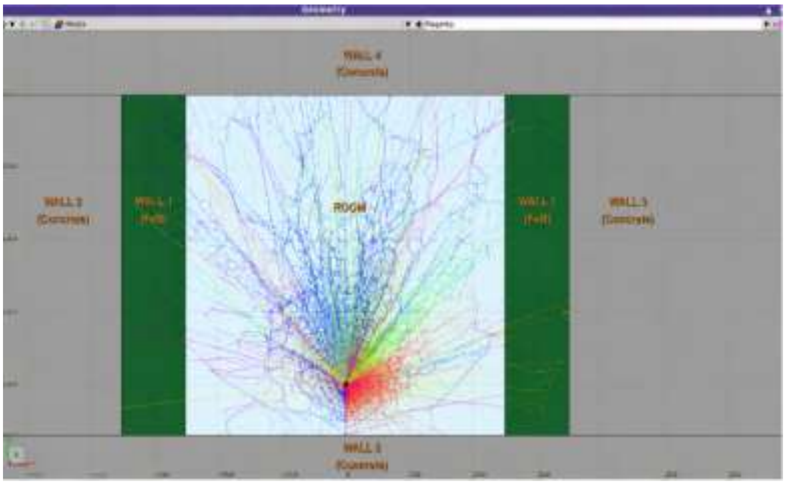

Figure 1. *Particle tracks generated by the interaction of a* ***250 MeV proton beam*** *with a copper target, as simulated using the* ***FLUKA MC*** *particle transport code. Secondary particles originating from the target region propagate through the tunnel air volume, the* ***FeB side shielding (Wall 1),*** *the* ***concrete side walls (Walls 2 and 3),*** *the* ***concrete roof (Wall 4),*** *and the* ***concrete floor (Wall 5).*** *The figure qualitatively illustrates the transport behavior and scattering characteristics of secondary particles within the multilayer shielding system.*

The computational domain was bounded by two concentric spherical surfaces centered at the same point in order to define the particle transport region. The inner sphere had a radius of **5900 cm,** whereas the outer sphere had a radius of **6000 cm.** The region between these two spheres was assigned as a **BLACKHOLE** region. This boundary condition ensured that particles leaving the computational domain were completely absorbed, thereby eliminating artificial backscattering from the outer boundary and improving the physical accuracy of the MC simulations.The developed computational geometry enabled a detailed investigation of the transport behavior of secondary particles generated by proton-target interactions within the **accelerator tunnel,** the **multilayer shielding system,** and the **surrounding natural soil.** Accordingly, the spatial characteristics of the radiation field and the shielding performance of the underground accelerator facility were evaluated with a high degree of physical fidelity.

4. Proton Beam Source and Physical Modeling

The primary particle source for the underground proton accelerator facility was defined using the **BEAM** and **BEAMPOS** cards available in the FLUKA MC code. A monoenergetic **250 MeV proton beam** was employed as the incident particle source. The beam was positioned at **(x, y, z) = (0, −1300, −500) cm** and directed along the positive *z*-axis with direction cosines of **(0, 0, 1).** Consequently, the incident protons propagated along the tunnel axis and interacted with the copper target located at approximately **(x, y, z) = (0, −1300, 0) cm,** where the production of secondary particles was initiated within the target volume.To represent a realistic operating condition for proton accelerator facilities, the simulations were performed assuming a **10 W point beam-loss** scenario. Under this condition, the proton beam intensity corresponded to approximately **2.496 × 10^{11} protons s^{-1}.** Proton-nucleus interactions within the copper target were modeled through intranuclear cascade and nuclear evaporation processes, leading to the production of a broad spectrum of secondary particles over a wide energy range. Among these, neutrons constituted the dominant component of the secondary radiation field, while photons, secondary protons, and other light charged particles also contributed to the overall radiation environment.Particle transport calculations were performed using the **DEFAULTS = SHIELDIN** physics option implemented in FLUKA. This predefined physics configuration simultaneously accounts for hadronic interactions, electromagnetic processes, intranuclear reactions, and low-energy neutron transport, thereby providing a physically consistent description of secondary particle production, scattering, moderation, and absorption within the shielding system. Consequently, the transport behavior of secondary particles and the moderation characteristics of neutrons within the multilayer shielding system and the surrounding natural soil were comprehensively evaluated under realistic underground operating conditions.

5. Material Composition and Properties

All materials used in the simulation geometry were implemented in FLUKA through the MATERIAL and COMPOUND cards and assigned to the corresponding regions using the ASSIGNMA card. The physical properties, elemental compositions, and shielding functions of the materials considered in the present study are summarized in Table 2.

Table 2. *Densities, chemical compositions, and principal physical roles in neutron transport and shielding performance of the materials used in the simulation geometry*

Material	Density (g/cm³)	Composition	Shielding Function/Role
Copper (Cu)	8.96	Cu	Primary target material; source of secondary particle production under proton interaction
Concrete	2.34	C, O, Si, Ca, H, Mg	Neutron moderation via elastic scattering (H-dominated)
Ferroboron (FeB)	7.15	Fe, B (~16.2 wt.% B)	Fast neutron energy degradation via inelastic scattering in Fe and thermal neutron absorption via $^{10}B(n,\alpha)^{7}Li$ reactions
Soil	1.90	O, Si, Al, Fe, Ca, Mg, Na, K	Combined neutron scattering and absorption
Air	0.00120484	N, O, Ar	Low-interaction transport medium

6. Underground Proton Accelerator Geometry and Shielding Configuration

The proton accelerator shielding geometry employed in this study was developed using the **CG** approach implemented in the FLUKA MC particle transport code. The computational domain was defined by two concentric spherical surfaces sharing the same center in order to confine particle transport. The inner sphere had a radius of **5900 cm**, whereas the outer sphere had a radius of **6000 cm**. The region between these two spheres was assigned as a **BLACKHOLE** region, ensuring that particles leaving the computational domain were completely removed from the simulation and preventing artificial backscattering from affecting the calculation results.To realistically represent an underground proton accelerator facility, the computational model was divided into two different environments by the **y = 0 cm** plane. The region above this plane was modeled as atmospheric air, while the region below was defined as the surrounding natural soil. Consequently, the accelerator tunnel was modeled as a realistic underground structure completely surrounded by natural soil.The accelerator tunnel was modeled as an air-filled region (TUNNEL) in which particle transport takes place. The tunnel dimensions extended from **−250 cm to +250 cm** along the *x*-axis, **−1400 cm to −900 cm** along the *y*-axis, and **−500 cm to +500 cm** along the *z*-axis, corresponding to an internal volume of approximately **5 m × 5 m × 10 m**. The proton beam was directed toward a copper target located within this air volume, where secondary particle production was initiated through proton–target interactions.The lateral shielding system was designed as a multilayer structure. On both sides of the tunnel, **100-cm-thick FeB shielding layers (Wall 1)** were positioned immediately adjacent to the tunnel air region. The left FeB layer extended from **x = −350 cm to −250 cm**, whereas the right FeB layer was defined between **x = +250 cm and +350 cm**. Owing to its boron content, the FeB shielding provides high absorption efficiency for thermal and epithermal neutrons, while the iron matrix contributes to the scattering and attenuation of high-energy neutrons.Outside the FeB layers, thick concrete walls were incorporated to provide additional biological shielding (**Walls 2 and 3**). The left concrete wall extended from **x = −2500 cm to −350 cm**, whereas the right concrete wall was defined between **x = +350 cm and +2500 cm**. Consequently, approximately **21.5 m** of concrete shielding was provided on each side of the accelerator tunnel. These concrete layers were designed to moderate fast neutrons, attenuate secondary gamma radiation, and reduce radiation dose levels outside the facility to values below the prescribed radiation protection limits.In the vertical direction, the tunnel was completely enclosed by concrete shielding. The roof shield (**Wall 4**) extended from **y = −900 cm to −100 cm** and was modeled as an **800-cm-thick** concrete layer. Similarly, the floor shield (**Wall 5**) extended from **y = −2200 cm to −1400 cm** and was also defined as an **800-cm-thick** concrete layer. Both the roof and floor shielding extended from **x = −2500 cm to +2500 cm** and **z = −500 cm to +500 cm**, thereby enclosing the tunnel along the vertical direction.The copper target was positioned approximately **100 cm above the tunnel floor**, near the geometric center of the tunnel. A monoenergetic **250 MeV proton beam** was directed toward the target, and the transport of neutrons and other secondary particles generated through nuclear interactions within the target was investigated throughout the multilayer shielding system.The resulting computational model consisted of an air-filled accelerator tunnel, FeB neutron shielding layers positioned on both sides of the tunnel, thick concrete biological shielding surrounding the FeB layers, concrete roof and floor shields, and the surrounding natural soil environment. This configuration enabled a comprehensive investigation of the transport and attenuation characteristics of neutrons and other secondary particles in both the horizontal (±*x*) and vertical (±*y*) directions under realistic underground proton accelerator conditions. The shielding geometry employed in this study is illustrated in **Figure 2**.

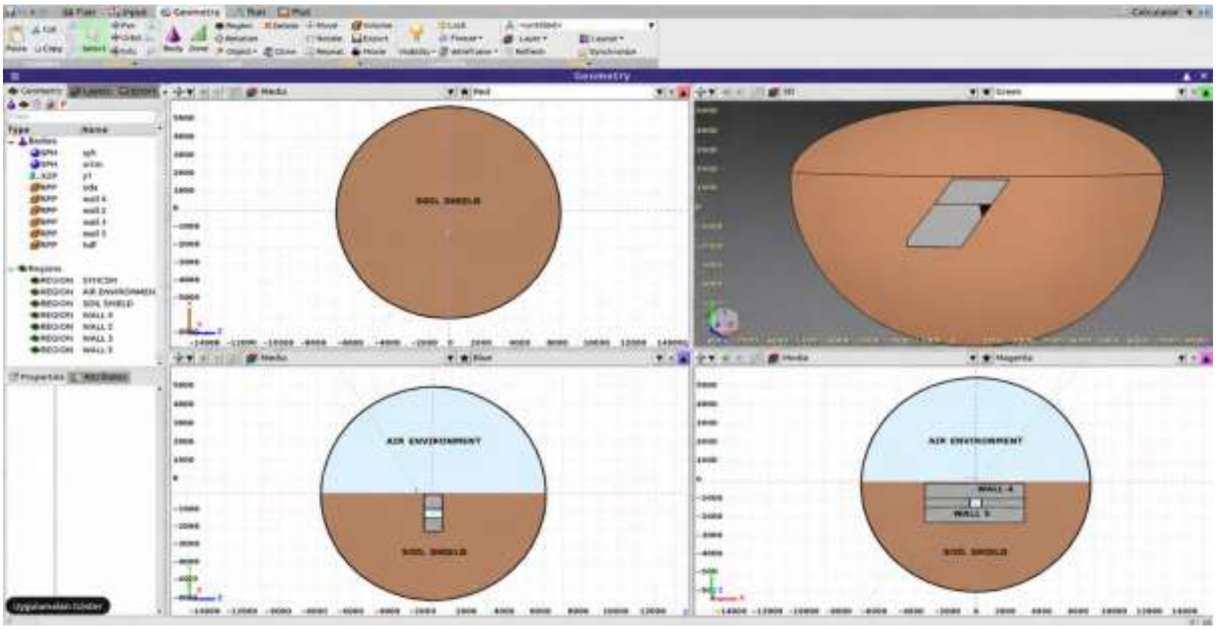

Figure 2. *Different views of the computational geometry of the 250 MeV underground proton accelerator employed in the FLUKA MC simulations. The figure illustrates the concentric spherical boundaries defining the computational domain, the air environment occupying the upper hemisphere, the natural soil region surrounding the underground facility in the lower hemisphere, and the accelerator tunnel embedded within the soil. The tunnel is enclosed by a multilayer shielding system consisting of an air-filled tunnel region, ferroboron side shielding (Wall 1), concrete side walls (Walls 2 and 3), a concrete roof shield (Wall 4), and a concrete floor shield (Wall 5). Front, three-dimensional, and sectional views are presented to illustrate the geometric configuration of the underground accelerator facility and its multilayer shielding system.*

7. Results and Discussion

The mechanisms of particle production resulting from the interaction of the proton beam with the copper target, particle absorption within the shielding system, and the behavior of low-energy neutrons were investigated in detail using FLUKA MC simulations. The results demonstrate that proton-target interactions generate not only secondary neutrons but also a complex mixed radiation field composed of secondary protons, photons, and other light charged particles. Therefore, particle transport was evaluated from three complementary perspectives: **(i)** secondary particle production, **(ii)** stopped particle distributions within the shielding system, and **(iii)** secondary particle production induced by low-energy neutron interactions. Since the particle yields span several orders of magnitude, all results are presented on a logarithmic scale.**Figure 3** illustrates the particle transport mechanisms resulting from the interaction of the **250 MeV proton beam** with the target and shielding materials from three different perspectives. Specifically, **(a)** secondary particles generated through inelastic nuclear reactions, **(b)** particles that lose all of their kinetic energy and are completely absorbed within the shielding system, and **(c)** secondary particles produced through low-energy neutron interactions are presented. These analyses provide a comprehensive understanding not only of the radiation field but also of the fundamental particle species contributing to it and their transport behavior within the multilayer shielding system. Because the particle production yields vary over several orders of magnitude, logarithmic scales were employed in all graphs to enable both dominant and low-yield particle species to be clearly visualized within the same figure.

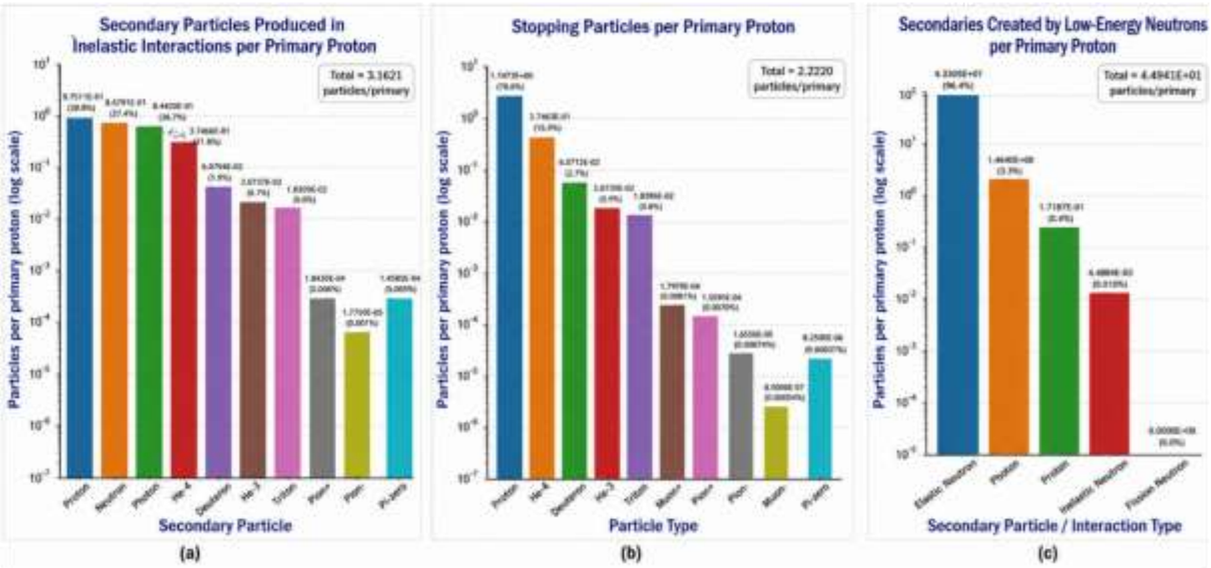

Figure 3. *Comparative illustration of the particle production processes occurring within the target and the multilayer shielding system of the* ***250 MeV proton accelerator. (a)*** *Distribution of secondary particles produced through inelastic nuclear reactions,* ***(b)*** *distribution of particles that lose all of their kinetic energy and are completely absorbed within the shielding materials, and* ***(c)*** *distribution of secondary particles generated by low-energy neutron interactions. Particle yields are expressed as the* ***number of particles produced per primary proton*** *and are presented on a logarithmic scale.*

Figure 3(a) presents the distribution of secondary particles produced through inelastic nuclear interactions. A total of 3.1621 secondary particles per primary proton were generated. Protons constituted the largest contribution (30.8%), followed by neutrons (27.4%) and photons (26.7%). Together, these three particle species account for approximately 85% of the total secondary particle yield, indicating that they dominate the radiation field generated by proton-target interactions. Alpha particles (11.8%), deuterons (1.9%), helium-3 nuclei (0.7%), and tritons (0.6%) were produced in considerably smaller quantities, whereas pion production was found to be negligible. These results indicate that the inelastic interactions of 250 MeV protons with the copper target predominantly produce protons, neutrons, and photons, which constitute the principal components governing radiation transport within the shielding system.Figure 3(b) shows the distribution of particles that were completely stopped within the shielding system after losing all of their kinetic energy. A total of 2.2220 particles per primary proton were absorbed, with protons accounting for the overwhelming majority (78.6%). Alpha particles represented the second largest contribution (16.9%), while deuterons (2.7%), helium-3 nuclei (0.9%), and tritons (0.8%) contributed to a much lesser extent. Muons and pions were observed at levels several orders of magnitude lower than those of the dominant particle species. The predominance of stopped protons indicates that charged particles lose their kinetic energy efficiently through ionization energy loss and nuclear interactions within high-density shielding materials such as concrete and FeB. Consequently, energy deposition within the shielding system is governed primarily by proton transport and absorption.Figure 3(c) presents the distribution of secondary particles generated through low-energy neutron interactions. The results demonstrate that low-energy neutron transport is dominated by elastic scattering processes. Elastically scattered neutrons reached 43.305 particles per primary proton, accounting for 96.4% of the total production. In comparison, photon production amounted to 1.464 particles per primary proton (3.3%), whereas proton production remained limited to 0.172 particles per primary proton (0.4%). Secondary particles generated through inelastic neutron reactions accounted for only approximately 0.01% of the total production, and no fission neutrons were observed. These findings indicate that, after being moderated within the shielding materials, neutrons continue to propagate predominantly through successive elastic scattering events, demonstrating that neutron transport is governed primarily by moderation processes. Furthermore, secondary photons generated through neutron capture and other neutron-induced reactions highlight the necessity of considering secondary gamma radiation in addition to neutron attenuation during shielding design.Overall, the three analyses presented in Figure 3 demonstrate that the radiation field generated by the 250 MeV proton beam is governed by multiple physical processes. Initially, proton-target interactions produce secondary particles dominated by protons, neutrons, and photons. Subsequently, charged particles gradually lose their kinetic energy and become fully absorbed within the shielding materials, whereas neutrons continue to propagate through repeated elastic scattering during the moderation process. These findings clearly indicate that effective shielding design for proton accelerator facilities should not rely solely on attenuating the primary proton beam but must also account for neutron moderation and the production of secondary gamma radiation. Therefore, the simultaneous evaluation of proton, neutron, and photon components is essential for optimizing multilayer shielding systems and ensuring radiation safety.

8. Conclusion

In this study, the secondary radiation field generated by the interaction of a **250 MeV proton beam** with a copper target in a **fully underground proton accelerator facility** was comprehensively investigated using the **FLUKA MC particle transport code.** In addition to secondary particle production, the distributions of particles completely absorbed within the shielding system and the behavior of low-energy neutron moderation were simultaneously evaluated, providing a comprehensive physical interpretation of radiation transport in underground proton accelerator facilities. Unlike previous studies that primarily focus on total dose or particle fluence, the present work contributes to a more detailed understanding of the fundamental physical processes governing the radiation field.The results demonstrate that the radiation field generated by proton-nucleus inelastic interactions is dominated by **protons, neutrons, and photons.** These three particle species constitute the majority of the total secondary particle production and represent the principal contributors to radiation transport within the accelerator tunnel. In contrast, alpha particles, deuterons, tritons, and other light ions contribute only a relatively small fraction of the secondary particle population. These findings indicate that hadronic interactions between **250 MeV protons** and the copper target predominantly produce protons, neutrons, and gamma photons, suggesting that these radiation components should be the primary consideration in shielding design.The analysis of particles completely stopped within the shielding system demonstrates that the multilayer **concrete-FeB** shielding structure effectively attenuates charged particles. The predominance of stopped protons indicates that ionization energy losses and nuclear interactions within the ferroboron and concrete layers significantly reduce the penetration range of charged particles. Consequently, the multilayer shielding system effectively controls not only neutron transport but also high-energy charged particles, thereby substantially reducing the amount of radiation that may escape the facility.The investigation of low-energy neutron interactions further revealed that neutron transport is governed predominantly by **elastic**

scattering. During the moderation process, neutrons gradually lose energy through successive elastic collisions, making neutron moderation the principal mechanism controlling neutron propagation within the shielding materials and the surrounding environment. In addition, secondary photons generated through neutron capture and other neutron-induced reactions demonstrate that neutron shielding simultaneously influences secondary gamma-ray production. Therefore, radiation protection assessments for proton accelerator facilities should consider not only neutron attenuation but also the coupled effects of neutron-photon interactions.The computational model developed in this study further demonstrates that the surrounding **natural soil** serves not only as a structural component but also as an additional natural shielding layer contributing to neutron moderation. Multiple scattering processes occurring within the soil modify the energy distribution of neutrons emerging from the engineered shielding system and consequently influence the spatial characteristics of the radiation field. These findings emphasize that the surrounding geological environment should be regarded as an integral component of shielding design for underground proton accelerator facilities.In conclusion, this study comprehensively investigated the fundamental physical mechanisms governing radiation transport in a **fully underground proton accelerator,** including **secondary particle production, charged-particle absorption, and low-energy neutron moderation.** The results demonstrate that the combined use of multilayer **FeB-concrete shielding** together with the surrounding natural soil provides effective attenuation of charged particles while simultaneously enhancing neutron moderation. These findings provide valuable guidance for the optimization of shielding systems, radiation protection analyses, and the safe design of future underground proton therapy facilities and accelerator-based research infrastructures.

Author Statements:

- **Ethical approval:** The conducted research is not related to either human or animal use.
- **Conflict of interest:** The authors declare that they have no known competing financial interests or personal relationships that could have appeared to influence the work reported in this paper

- **Acknowledgement:** The authors declare that they have nobody or no-company to acknowledge.

- **Author contributions:** The authors declare that they have equal right on this paper.

- **Funding information:** The authors declare that there is no funding to be acknowledged.

- **Data availability statement:** The data that support the findings of this study are available on request from the corresponding author. The data are not publicly available due to privacy or ethical restrictions.

References

[1] Sasamoto, N., Nakashima, H., Hirayama, H., Shibata, T., 2002. Status on shielding design study for the high-intensity proton accelerator facility. *Journal of Nuclear Science and Technology* 39 (Suppl. 2), 1264–1267. https://doi.org/10.1080/00223131.2002.10875334

[2] Mueller, M.J., Stevenson, G.R., 2005. Shielding design of an underground experimental area at Point 5 of the CERN Super Proton Synchrotron (SPS). *Radiation Protection Dosimetry* 115 (1-4), 181-186. https://doi.org/10.1093/rpd/nci178

[3] DiJulio, D.D., Eshraqi, M., Hees, W., Hinrichsen, Y., Klinkby, E., Lundmark, A., Muhrer, G., Noll, D., 2022. Radiation transport calculations for the European Spallation Source accelerator environment. *Proceedings of the 14th International Conference on Radiation Shielding (ICRS-14/RPSD-2022)*, Seattle, WA, USA. https://doi.org/10.13182/ICRSRPSD22-39130

[4] Sariyer D., Yıldırım E., 2026. A hybrid Monte Carlo–machine learning framework for high-energy neutron shielding using boron-enhanced concrete. Int. J. Comput. Exp. Sci. Eng. 12 (1), 447-461. https://doi.org/10.22399/ijcesen.48827

[5] Sarıyer, D., Yıldırım, E., 2026. Multidirectional neutron shielding analysis and surrogate-based optimization of multilayer ferroboron for a 1000 MeV proton accelerator. Annals of Nuclear Energy, 238, Article No. 112537. https://doi.org/10.1016/j.anucene.2026.112537

[6] Sarıyer, D., Gökcan, A.O., 2026. *A hybrid Monte Carlo-machine learning framework for neutron dose attenuation modeling in layered iron-concrete shields of a 1000 MeV proton accelerator*. Annals of Nuclear Energy, 238, Article No. 112572. https://doi.org/10.1016/j.anucene.2026.112572

[7] Gökcan A.O., Sariyer D., 2026. High-energy neutron shielding analysis using curve fitting and machine learning: A Monte Carlo-based study in concrete and ferro-boron configurations. Ann. Nucl. Energy 232, 112244. https://doi.org/10.1016/j.anucene.2026.112244

[8] Sariyer, D., 2026. Hybrid machine learning-Monte Carlo approach for neutron shielding in high-energy proton facilities. *Journal of Subatomic Particles and Cosmology* 5, 100309. https://doi.org/10.1016/j.jspc.2026.100309.
[9] CERN, *Accelerator Applications and Technologies Reports*, Geneva.
[10] Alhazmi, N.K., Alanazi, S.D., Alrowily, H.S.A., Alkhamsan, K.F., Al-Rashidi, F.A.D., Mohammed, A.-S.S., Khalaf, A.M., Alshammari, S.F.N., Alzaidi, A.A., Alshammari, F.T.N., AlQusayri, A.A., 2024. Radiation safety compliance and protective practices among radiologic technologists. *International Journal of Computational and Experimental Science and Engineering* 10 (4). https://doi.org/10.22399/ijcesen.4664
[11] Sarıyer, D., & Küçer, R. 2014. Determination of the shielding thickness required for controlled areas in proton accelerators using the FLUKA Monte Carlo code. *Suleyman Demirel University Journal of Natural and Applied Sciences*, 9:142-149.
[12] Sarıyer, D., Erbil, M.E., 2026. Comparative analysis of secondary particle production and spatial dose distributions in multilayer concrete-iron shielding systems for a 50 MeV proton accelerator using FLUKA. *International Journal of Computational and Experimental Science and Engineering (IJCESEN)* 12 (1), 1485-1495. https://doi.org/10.22399/ijcesen.5083
[13] Sarıyer, D., Küçer, R., 2014. Determination of concrete and soil shielding thicknesses for 100-250 MeV proton accelerators using the FLUKA Monte Carlo code. *SDU Journal of Science* 9(1), 117-124.
[14] Aydın, H., Süsoy Doğan, G., Tekin, H.O., Şen Baykal, D., İltuş, Y.C., 2025. Examining the neutron and gamma attenuation characteristics of various amorphous structures with bioactive properties. *International Journal of Computational and Experimental Science and Engineering* 11 (3). https://doi.org/10.22399/ijcesen.2176
[15] Dinter, H., Tesch, K., Dworak, D., Doses due to neutrons and charged particles in the angular range 10° to 170° behind concrete shield of high-energy proton accelerators, *Nuclear Instruments and Methods in Physics Research Section A: Accelerators, Spectrometers, Detectors and Associated Equipment*, 384(2–3), 539-543, 1997. https://doi.org/10.1016/S0168-9002(96)00921-
[16] Sarıyer, D., Yıldırım, E., 2026. Rapid secondary neutron dose estimation in proton accelerators using FLUKA and machine learning. *Süleyman Demirel University Faculty of Arts and Sciences Journal of Science* 21 (1), 1–18. https://doi.org/10.29233/sdufeffd.1783848
[17] Ferrari, A., Sala, P.R., Fasso, A., Ranft, J., 2005. FLUKA: A multi-particle transport code, CERN-2005-10.
[18] Battistoni, G., Boehlen, T.T., Cerutti, F., Chin, P.W., Esposito, L.S., Fassò, A., Ferrari, A., Lechner, A., Empl, A., Mairani, A., Mereghetti, A., Garcia Ortega, P., Ranft, J., Roesler, S., Sala, P.R., Vlachoudis, V., Smirnov, G., 2015. *Overview of the FLUKA code*. Annals of Nuclear Energy, 82, 10-18. https://doi.org/10.1016/j.anucene.2014.11.007
[19] Böhlen, T.T., Cerutti, F., Chin, M.P.W., Fassò, A., Ferrari, A., Ortega, P.G., Mairani, A., Sala, P.R., Smirnov, G., Vlachoudis, V., 2014. *The FLUKA Code: Developments and Challenges for High Energy and Medical Applications*. Nuclear Data Sheets, 120, 211–214. https://doi.org/10.1016/j.nds.2014.07.049
[20] Sarıyer, D., 2025. FLUKA Monte Carlo assessment of Fe_2B-based shielding materials for high-energy proton accelerator environments. International Journal of Computational and Experimental Science and Engineering 11, 9864-9869. https://doi.org/10.22399/ijcesen.4544
[21] Sarıyer, D., 2020. *Investigation of Neutron Attenuation through FeB, Fe_2B and Concrete*. Acta Physica Polonica A, 137(4), 539-542. https://doi.org/10.12693/APhysPolA.137.539
[22] Sarıyer, D., Küçer, R., Küçer, N., 2015. *Neutron Shielding Properties of Concrete and Ferro-Boron*. Acta Physica Polonica A, 128(2-B), B201-B202. https://doi.org/10.12693/APhysPolA.128.B-201
[23] Sarıyer, D., & Küçer, R., 2013. Determination of shielding thicknesses for different materials in proton accelerators using an analytical method. SDU Journal of Science (E-Journal), 8(1):100-105.
[24] Günoğlu, K., & Akkurt, İ. (2024). *Gamma-ray attenuation properties carbide compounds (WC, Mo_2C, TiC, SiC, B_4C) using Phy-X/PSD software*. International Journal of Applied Sciences and Radiation Research, 1(1). https://doi.org/10.22399/ijasrar.6
[25] Sarıyer, D., Küçer, R., 2018. Double-layer neutron shield design as neutron shielding application. *AIP Conference Proceedings* 1935, 180004. https://doi.org/10.1063/1.5026020
[26] Yani, S., Rahma, W., Sumaryada, T., Endarko, Haryanto, F., Tai, D.T., Omer, H., Tamam, N., Sulieman, A., Dirgayussa, I.G.E., Nuraeni, N., 2026. Optimization of proton radiation shielding using multilayer concrete-iron-polyethylene barriers: A PHITS Monte Carlo study. Radiat. Phys. Chem. 240, 113422. https://doi.org/10.1016/j.radphyschem.2025.11342
[27] Aliyah, F., 2024. *Multi-layer Radiation Shielding Design for Compact Proton Therapy System Using Monte Carlo Simulation*. Master's Thesis, Universiti Sains Malaysia (USM), Malaysia.
[28] Fang, P.W., Hsieh, Y.I., Shiau, A.C., Sheu, R.J., 2025. Studies on shielding and activation levels in a concrete-iron-concrete sandwich structure wall in the CMUH proton therapy facility. *Health Physics* 129 (4), 307–314. https://doi.org/10.1097/HP.0000000000001943